Arabidopsis Homologs of the *Petunia HAIRY MERISTEM* Gene Are Required for Maintenance of Shoot and Root Indeterminacy[1][C][W][OA]

Eric M. Engstrom*, Carl M. Andersen, Juliann Gumulak-Smith, John Hu, Evguenia Orlova, Rosangela Sozzani, and John L. Bowman

Biology Department, College of William and Mary, Williamsburg, Virginia 23187–8795 (E.M.E., C.M.A., J.G.-S., J.H., E.O.); Department of Biology and Institute for Genome Sciences and Policy Center for Systems Biology, Duke University, Durham, North Carolina 27708 (R.S.); and School of Biological Sciences, Monash University, Clayton Campus, Melbourne, Victoria 3800, Australia (J.L.B.)

Maintenance of indeterminacy is fundamental to the generation of plant architecture and a central component of the plant life strategy. Indeterminacy in plants is a characteristic of shoot and root meristems, which must balance maintenance of indeterminacy with organogenesis. The *Petunia hybrida HAIRY MERISTEM* (*HAM*) gene, a member of the GRAS family of transcriptional regulators, promotes shoot indeterminacy by an undefined non-cell-autonomous signaling mechanism(s). Here, we report that Arabidopsis (*Arabidopsis thaliana*) mutants triply homozygous for knockout alleles in three Arabidopsis *HAM* orthologs (*Atham1,2,3* mutants) exhibit loss of indeterminacy in both the shoot and root. In the shoot, the degree of penetrance of the loss-of-indeterminacy phenotype of *Atham1,2,3* mutants varies among shoot systems, with arrest of the primary vegetative shoot meristem occurring rarely or never, secondary shoot meristems typically arresting prior to initiating organogenesis, and inflorescence and flower meristems exhibiting a phenotypic range extending from wild type (flowers) to meristem arrest preempting organogenesis (flowers and inflorescence). *Atham1,2,3* mutants also exhibit aberrant shoot phyllotaxis, lateral organ abnormalities, and altered meristem morphology in functioning meristems of both rosette and inflorescence. Root meristems of *Atham1,2,3* mutants are significantly smaller than in the wild type in both longitudinal and radial axes, a consequence of reduced rates of meristem cell division that culminate in root meristem arrest. *Atham1,2,3* phenotypes are unlikely to reflect complete loss of HAM function, as a fourth, more distantly related Arabidopsis *HAM* homolog, *AtHAM4*, exhibits overlapping function with *AtHAM1* and *AtHAM2* in promoting shoot indeterminacy.

Indeterminate growth, the continuing generation and growth of organs and tissues throughout the life cycle of an organism, is a fundamental component of postembryonic plant development. Vascular plants grow discontinuously throughout their life spans, repeatedly initiating new shoot and root systems. This capacity for growth throughout the life span permits plants to adaptively regulate their growth patterns in response to dynamic environments, since, as sessile organisms, they cannot relocate in response to environmental stressors. Indeterminate growth is also a fundamental aspect of the "life strategy" of vascular plants, endowing woody perennials with the capacity for individuals to achieve life spans of thousands of years.

In plants, indeterminate growth is the function of plant meristems. Lateral organs (leaves and floral organs) and stems are derived from shoot meristems, located at shoot apices. Root meristems, internal meristems located immediately above the columella of root apices, generate the radially organized tissues of the root. The primary shoot apical and root apical meristems arise during embryogenesis, while secondary meristems arise de novo during postembryonic development (McConnell and Barton, 1998; Laskowski et al., 2008). Meristems must balance two competing functions: specification of determinate tissues, which reduces the pool of undifferentiated and pluripotent cells; and maintenance of indeterminacy, which requires the retention of a pool of undifferentiated and pluripotent cells from which cells lost to differentiating tissues may be replaced. The dual-functional nature of meristems is reflected in meristem structure. Small populations of internally located cells function

[1] This work was supported by the College of William and Mary (institution paper no. 204), by the U.S. Department of Agriculture, Cooperative Research, Education, and Extension Service, National Research Initiative Competitive Grants Program (grant no. 2003–02600 to E.M.E.), and by a Howard Hughes Medical Institute grant to J.H. through the Undergraduate Biological Sciences Education Program to the College of William and Mary.

* Corresponding author; e-mail emengs@wm.edu.

The author responsible for distribution of materials integral to the findings presented in this article in accordance with the policy described in the Instructions for Authors (www.plantphysiol.org) is: Eric M. Engstrom (emengs@wm.edu).

[C] Some figures in this article are displayed in color online but in black and white in the print edition.

[W] The online version of this article contains Web-only data.

[OA] Open Access articles can be viewed online without a subscription.

www.plantphysiol.org/cgi/doi/10.1104/pp.110.168757

as organizing centers, signaling to maintain an undifferentiated state in adjoining meristematic cells. In shoot meristems, undifferentiated cells are located immediately above the organizing center and constitute the "central zone," while in the root, undifferentiated initial cells surround the organizing center. Cells displaced from the shoot meristem central zone or root meristem initial zone ultimately undergo differentiation (Dinneny and Benfey, 2008).

Stuurman et al. (2002) identified the HAIRY MERISTEM (HAM) protein, a member of the GRAS family of transcription factors, as a component of a novel non-cell-autonomous signaling pathway maintaining shoot indeterminacy in *Petunia hybrida*. Wild-type *Petunia* plants produce as many as 19 leaves before transitioning to flowering. *ham* mutants exhibit cessation of lateral organ and stem production (meristem arrest) and differentiation of the shoot apical meristem into stem tissue following the production of six to 14 leaves (Stuurman et al., 2002). Arrest in lateral organ production in *ham* mutants is similar to the *wus* phenotype in both Arabidopsis (*Arabidopsis thaliana*) and *Petunia*, but differentiation of the shoot meristem is unique to *ham* mutants (Laux et al., 1996; Stuurman et al., 2002). *HAM* is expressed in the provasculature and internal regions of the meristem subtending initiating lateral organs. An upward expansion of *HAM* expression occurs below sites of lateral organ initiation and continues into the emerging organ, remaining contiguous with *HAM* expression in the stem provasculature. *HAM* expression is not reported in central zone meristem cells, and *HAM* expression in meristem L3 cells is sufficient to restore meristem function. Collectively, these data were interpreted by Stuurman and colleagues (2002) as consistent with HAM promoting shoot indeterminacy via a non-cell-autonomous pathway.

Arabidopsis orthologs of *Petunia HAM* are probable endogenous targets of posttranscriptional degradation by microRNAs (MIRs) 170 and 171 (Llave et al., 2002). MIRs are small (21–24 nucleotide) RNAs produced from endogenously encoded RNA precursors (miRs) that act to direct posttranscriptional silencing of target mRNAs (Baulcombe, 2004; Brodersen and Voinnet, 2006). Within the past decade, posttranscriptional regulation of expression by MIRs has emerged as a major regulatory mode of meristem regulation and organ patterning. mRNA of two Arabidopsis *HAM* orthologs is shown to be cleaved at the MIR171/170-binding site in inflorescence tissue, coincident with the highest detected levels of miR171 (Llave et al., 2002; Parizotto et al., 2004). Additional support for endogenous regulation of Arabidopsis *HAM* orthologs by MIR170/171 arises from the observation that mRNA levels of one ortholog are elevated in mutant plants in which MIR production is impaired (Vazquez et al., 2004).

Continuing genetic analyses of *HAM* function in regulating indeterminacy would be greatly furthered by the identification and characterization of Arabidopsis *ham* mutants. In this study, we present the results of a detailed characterization of shoot and root phenotypes resulting from loss of function in Arabidopsis homologs of *Petunia HAM*. We show that while the four Arabidopsis *HAM* homologs span the range of flowering plant *HAM* diversity, all four Arabidopsis *HAM* homologs promote shoot indeterminacy. Arabidopsis orthologs of *Petunia HAM* are shown to regulate root indeterminacy as well, placing *HAM* orthologs into a comparatively small set of meristem regulators that function in the regulation of both shoot and root meristems. These results expand upon our understanding of HAM protein function in postembryonic development and provide a foundation for both future genetic analyses of *HAM* function and characterization of the molecular phenotype of *ham* mutants.

RESULTS

HAM Genes Underwent Expansion of Homolog Diversity and Elevated Rates of Evolution in Flowering Plants

Earlier phylogenetic analyses demonstrate that *HAM* genes have a long evolutionary history in land plants. *HAM* homologs are present in the genomes of representative species from the moss, lycophyte, and fern lineages (Floyd and Bowman, 2007; E.M. Engstrom, unpublished data). Among completely sequenced plant genomes, the moss *Physcomitrella patens* and the lycophyte *Selaginella moellendorffii* each possesses a single *HAM* homolog, while the flowering plants rice (*Oryza sativa*) and Arabidopsis each possesses four *HAM* homologs (Bolle, 2004; Tian et al., 2004; E.M. Engstrom, unpublished data). Expansion of homology diversity suggests the acquisition of new functions and/or functional subspecialization (Lynch, 2007). To determine whether the expansion of *HAM* homologs observed in rice and Arabidopsis is broadly characteristic of flowering plants as a group, or alternatively is a trait that arose independently in discrete lineages within flowering plant diversity, we undertook a phylogenetic analysis of HAM proteins from 23 flowering plants, two gymnosperms, and single representative species from the moss, fern, and lycophyte lineages (Supplemental Table S1). Despite the likelihood that this analysis does not include the complete set of *HAM* homologs from species for which complete genomic sequence is not yet available, expansion and diversification of *HAM* homologs are evident across the monocot and core eudicot lineages, with as many as eight *HAM* genes in the poplar (*Populus* spp.) and soybean (*Glycine max*) genomes (Fig. 1A). Diversification of flowering plant *HAM* genes initiated with a split into two major clades (HAM I and HAM II) prior to the divergence of the monocot and core eudicot lineages. Core eudicots have retained *HAM* homologs from both clades, while monocots retain *HAM* homologs of the HAM II clade only. The rate of amino acid sequence change in flowering plant HAM homologs is

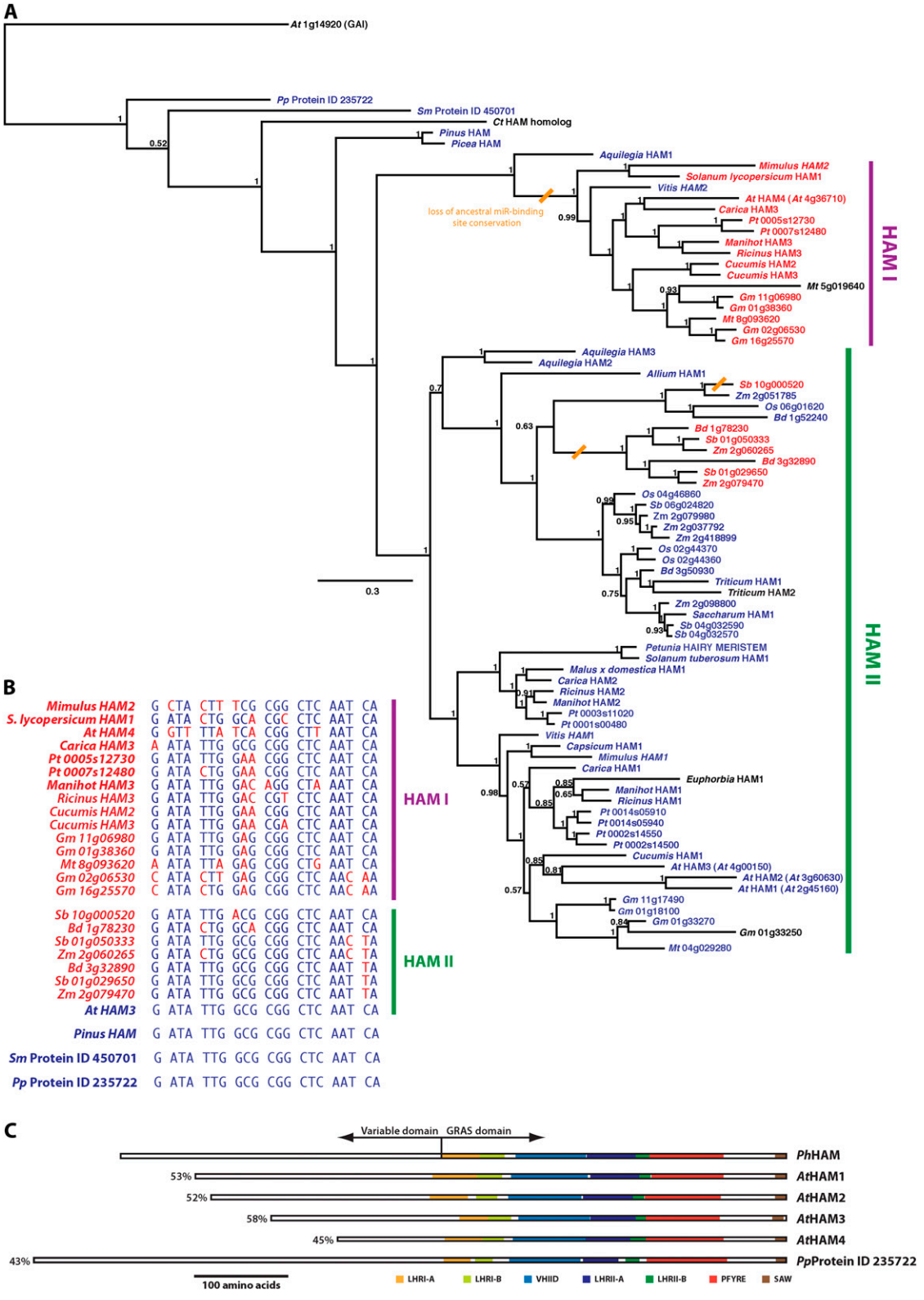

Figure 1. Arabidopsis *HAM* homolog proteins occupy two distantly related flowering plant HAM protein clades, characterized by retention or loss of microRNA regulation. A, Phylogeny of HAM proteins. The rooted phylogram shows aligned protein sequences of 78 HAM proteins from 23 flowering plant species, the gymnosperms *Pinus* and *Picea*, the fern *Ceratopteris thalictroides*, the lycophyte *S. moellendorffii*, and the moss *P. patens* (Supplemental Table S1), derived from Bayesian inference. Support values, indicated to the left of nodes, denote posterior probabilities. The scale bar indicates substitutions per site. The

significantly elevated relative to nonflowering plants, suggesting the evolution of novel *HAM* gene functions in response to selective pressures specific to flowering plants (Fig. 1A).

Arabidopsis *HAM* Homologs Span Flowering Plant *HAM* Diversity

Three Arabidopsis *HAM* homologs, *AtHAM1* (At2g45160), *AtHAM2* (At3g60630), and *AtHAM3* (At4g00150), were previously identified as targets of posttranscriptional regulation by MIRs 170/171 (Llave et al., 2002; Rhoades et al., 2002). The MIR170/171-binding sequence, 5′-GATATTGGCGCGGCTCAATCA-3′, is perfectly conserved within HAM II eudicots, and within moss, lycophyte, and gymnosperm *HAM* homologs, strongly indicating that MIR regulation is an ancestral trait of *HAM* genes that arose before the divergence of the moss and vascular plant lineages (Fig. 1, A and B; Axtell et al., 2007). AtHAM1, AtHAM2, and AtHAM3 are located in the HAM II clade, along with *Petunia* HAM, and are more closely related to one another than to other members of the HAM II clade. *AtHAM1*, *AtHAM2*, and *AtHAM3*, therefore, appear to be paralogs derived from a relatively recent set of gene duplication events and are orthologs of *Petunia HAM*. AtHAM1, AtHAM2, and AtHAM3 exhibit comparable levels of protein sequence identity over their alignable GRAS domains with *Petunia* HAM, ranging from 52% for AtHAM2 to 58% for AtHAM3 (Fig. 1C).

The fourth *HAM* homolog, *AtHAM4* (At4g36710), resides in the HAM I clade (Fig. 1A). With the exceptions of *HAM* homologs from *Aquilegia* and *Vitis*, all members of the HAM I clade for which complete sequence is available exhibit lack of conservation of the ancestral MIR-binding sequence. The *AtHAM4* sequence homologous to the MIR170/171-binding sequence diverges from the ancestral *HAM* MIR-binding sequence at six of 21 nucleotides, making it highly unlikely that *AtHAM4* is regulated by MIR170/171 (Fig. 1B). Protein sequence identity of AtHAM4 to *Petunia* HAM is comparable in degree to the much more distantly related *Physcomitrella* HAM homolog (Fig. 1C).

AtHAM1, *AtHAM2*, and *AtHAM3* Are Expressed in Apical Meristems and in Differentiating and Mature Tissues of Both Shoot and Root

Determining the domains of *AtHAM* ortholog expression must account for MIR170/171-mediated posttranscriptional regulation. Promoter::reporter fusion constructs generally do not reflect posttranscriptional regulation, while RNA detection methods optimally should distinguish between full-length mRNA and products of MIR-directed cleavage. Llave et al. (2002) report the expression of full-length *AtHAM2* and *AtHAM3* in leaf, stem, and inflorescence tissue, detected by RNA gel blot (Llave et al., 2002). Expanding upon this work, we undertook to amplify segments of *HAM* orthologs *AtHAM1*, *AtHAM2*, and *AtHAM3* by reverse transcription (RT)-PCR from cDNA derived from entire vegetative shoots, mature rosette leaves, inflorescence stem and flowers, fully expanded but unripe siliques, and roots using primer sets that discriminate full-length transcripts from MIR170/171 cleavage products. *AtHAM1*, *AtHAM2*, and *AtHAM3* are consistently amplified from all tissues surveyed (Supplemental Fig. S1), consistent with all three Arabidopsis *HAM* orthologs functioning in root, vegetative shoot, and reproductive shoot tissues.

Petunia HAM gene expression in both vegetative and inflorescence shoot meristems is associated most strongly with differentiating organ anlagen and provasculature, with expression highly reduced or excluded from central and apical meristem zones, and extending into the interior tissues of developing lateral organ primordia (Stuurman et al., 2002). To determine if and to what extent the patterns of expression of Arabidopsis *HAM* orthologs are similar to that of *Petunia HAM*, we performed in situ hybridization experiments to determine the localization of *AtHAM1* expression in shoot apices of 12-d-old wild-type seedlings. In situ hybridization reveals the expression of *AtHAM1* in young leaves and differentiating leaf primordia, with the level of expression elevated in interior regions of leaf primordia (Fig. 2A). Within the shoot meristem, *AtHAM1* expression exhibits a gradient of expression, with the lowest level of expression in the meristem L1 layer and increasing expression pro-

Figure 1. (*Continued.*)
tree is rooted with a set of 12 DELLA proteins, although for visual simplicity only the Arabidopsis GA-INSENSITIVE protein is shown. Proteins encoded by genes that retain a perfectly conserved MIR-binding sequence are colored blue; proteins encoded by genes in which the MIR-binding sequence is imperfectly conserved are colored red. The phylogenetic locations of inferred losses in MIR-binding sequence conservation are indicated by slanted orange bars. The two largest monophyletic clades of flowering plant HAM proteins are designated HAM I and HAM II. B, Evolution of the MIR-binding sequence in flowering plant *HAM* genes. The MIR170/171-binding site sequence of *AtHAM3* (Llave et al., 2002) is shown, along with the homologous sequences of HAM I and HAM II genes that deviate from the ancestral MIR-binding sequence and the conserved MIR-binding sequences of *Pinus*, *Selaginella*, and *Physcomitrella*. Nucleotides conserved with the ancestral MIR-binding sequence are colored blue; nucleotides that deviate from the ancestral MIR-binding sequence are colored red. C, Relative amino acid sequence identity of Arabidopsis homologs to *Petunia* HAM. A more distantly related HAM homolog from *Physcomitrella* is included for comparison. Percentage of pairwise amino acid identity between the aligned C-terminal GRAS domain with *Petunia* HAM, excluding alignment gaps, is indicated to the left of each Arabidopsis and *Physcomitrella* homolog. Indicated GRAS domain subunits follow the criteria proposed by Tian et al. (2004).

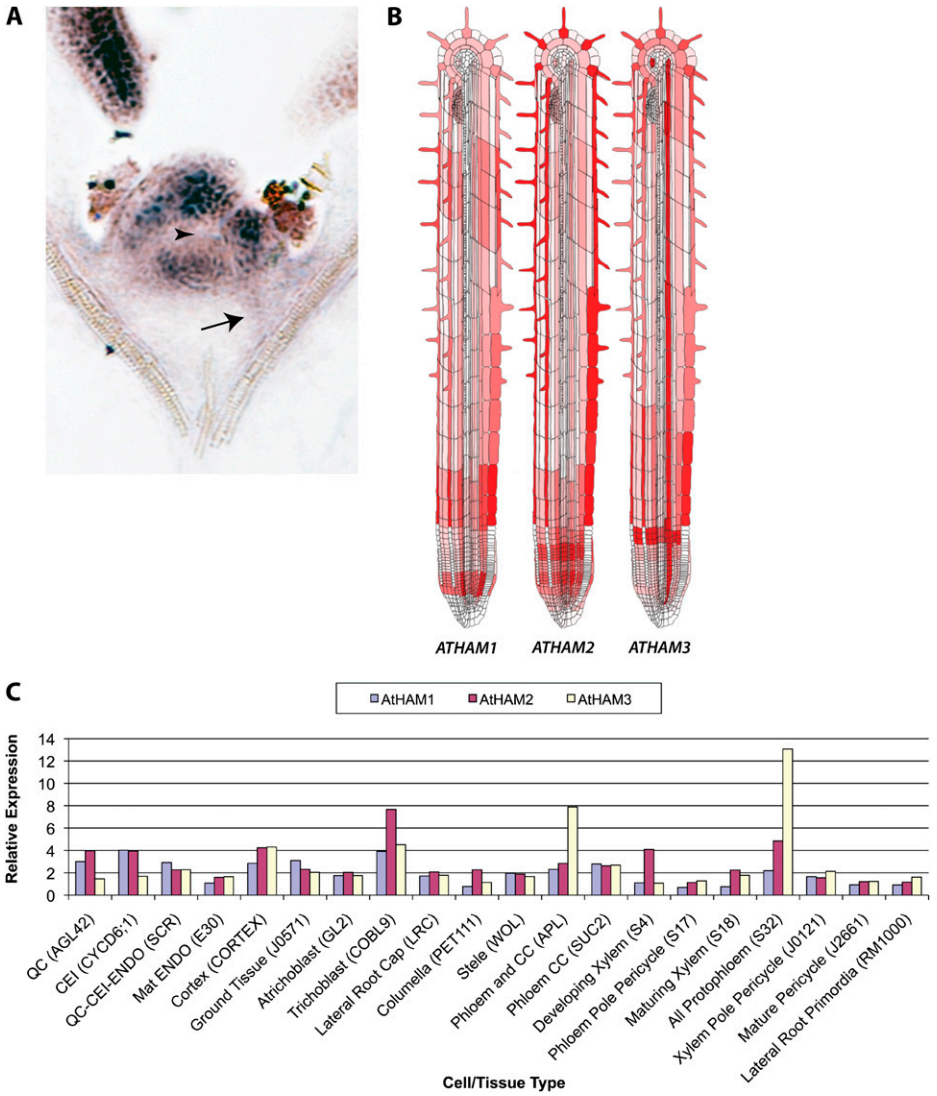

Figure 2. Arabidopsis *HAM* orthologs are expressed in meristematic and differentiated tissues of both the shoot and the root. A, In situ localization of *AtHAM1* in a L*er* shoot apex in a median longitudinal section. The L1 meristem cell layer is indicated with the arrowhead. A strong signal is consistently detected in lateral organ primordia. Signal is also detected in the meristem itself, with the highest level of signal present in the basal meristem regions and reduced or no signal in evidence in the uppermost cell layers of the central meristem region. *AtHAM1* expression in the provasculature is indicated with the arrow. B, Expression maps of Arabidopsis *HAM* orthologs in root tissue, from The Arabidopsis Gene Expression Database (Birnbaum et al., 2003; Brady et al., 2007). Darker hues reflect higher relative expression levels within the root and between *AtHAM* orthologs. C, Relative expression levels of *AtHAM* orthologs in specific cell and tissue types. Values graphed are means of three replicates of normalized expression levels derived from mixed-model ANOVA analysis profiled by microarray profiling. Specific cell and tissue types are indicated, along with the marker employed to delineate spatial expression patterns in parentheses. Data shown are derived from the analysis reported by Brady et al. (2007), with the exceptions of cortex/endodermal initial (CEI; Sozzani et al., 2010) and mature endodermis (Mat ENDO; Carlsbecker et al., 2010). QC indicates the quiescent center.

gressing downward into L3 meristem cells. Immediately basal of the shoot meristem boundary, there is a sharp decrease or cessation in *AtHAM1* expression, though more laterally, *AtHAM1* expression is maintained in differentiating stem provasculature.

HAM genes are expressed in roots of both *Petunia* and Arabidopsis (Stuurman et al., 2002; Supplemental Fig. S1). To determine the expression patterns of *AtHAM* orthologs in the root at high spatial resolution, we examined transcriptional profiles of individual root cell types for all three Arabidopsis *HAM* orthologs, utilizing AREX, the Arabidopsis Gene Expression Database (Birnbaum et al., 2003; Brady et al., 2007; Carlsbecker et al., 2010; Sozzani et al., 2010). Root expression patterns of *AtHAM1*, *AtHAM2*, and *AtHAM3* share considerable overlap with regard to the

cell types and tissues in which they are expressed, but they exhibit ortholog-specific relative expression levels (Fig. 2, B and C). Within the meristem region, all three orthologs are expressed in quiescent center, cortex/endodermal initials, and endodermis, cortex, and stele cell files. In differentiating and mature tissues, all three orthologs are expressed in columella, root cap, epidermis, cortex, endodermis, and stele. Moreover, all three orthologs exhibit a striking pattern of expression in the epidermis, with significantly elevated expression in trichoblast epidermal cell files relative to atrichoblast epidermal cell files in differentiating and mature root. This pattern is inverted within the meristem, with atrichoblast cell files exhibiting *AtHAM* ortholog expression, while trichoblast cell files show low or no *AtHAM* ortholog expression. Ortholog-specific differences in relative expression levels are greatest in differentiating and mature trichoblast, where *AtHAM2* predominates, in phloem and protophloem, where *AtHAM3* predominates, and in developing xylem, where *AtHAM2* again predominates. Within the meristem region, *AtHAM3* expression is elevated relative to *AtHAM1* and *AtHAM2* in a radial root section three cells in height, at the transition zone between the root meristem and elongation zone. *AtHAM2* expression is elevated relative to *AtHAM3* in a longer bipartite cross section of the root meristem, immediately adjacent to and below the band of elevated *AtHAM3* expression, while *AtHAM1* expression is elevated relative to *AtHAM3* in a cross section of root meristem located several cells above the quiescent center and overlapping with the band of elevated *AtHAM2* expression.

Atham1,2,3 Mutants Exhibit Abnormalities in Postembryonic Shoot Development, Including Aberrant Phyllotaxis, Altered Meristem and Leaf Morphology, and Loss of Shoot Indeterminacy

Our phylogenetic analysis of HAM proteins suggests that the *Petunia ham* phenotype of shoot apical meristem arrest and differentiation is most likely to be recapitulated in Arabidopsis by loss-of-function mutants of *AtHAM1*, *AtHAM2*, and *AtHAM3*. We identified insertional mutant alleles, predicted to confer complete loss of function, for *AtHAM1*, *AtHAM2*, and *AtHAM3* (Supplemental Fig. S2A). Consistent with the insertions generating null loss-of-function (knockout) alleles, wild-type transcripts are not detectable by RT-PCR in homozygous insertion allele backgrounds (Fig. 3, A and B). As *Atham2-1* and *Atham3-1* both reside in the Landsberg *erecta* (L*er*) background, we elected to use the L*er* genotype as a wild-type reference in our characterizations of *Atham1,2,3* mutants.

Single *AtHAM* knockout mutants and all three combinations of *AtHAM* double mutants (*Atham1,2*, *Atham1,3*, and *Atham2,3* mutants) do not notably differ in their shoot phenotypes from the wild type (data not shown), consistent with considerable functional redundancy among *AtHAM* orthologs. Plants homozygous for knockout alleles in all three *AtHAM* orthologs (*Atham1,2,3* mutants) exhibit a spectrum of abnormal shoot phenotypes. *Atham1,2,3* mutants do not exhibit notable embryogenesis defects, as gauged by normal development of hypocotyl, cotyledons, and root and shoot meristems (Fig. 3C). The earliest evident phenotypic abnormalities in *Atham1,2,3* mutants are deviations from the normal phyllotactic patterning of rosette leaves, which frequently are apparent as early as the emergence of the third and fourth leaves (Fig. 3D). At this stage in development, examination of sectioned shoot apices reveals that *Atham1,2,3* shoot apical meristems are consistently broader and flatter than in the wild type (mild fasciation), although overall meristem size is not appreciably different (Fig. 3E). Fully expanded rosette leaves of *Atham1,2,3* mutants typically exhibit less pronounced laminar growth and more pronounced leaf serration relative to wild-type expanded rosette leaves (Fig. 3F). Examination of the adaxial and abaxial epidermis of wild-type and *Atham1,2,3* expanded rosette leaves by scanning electron microscopy reveals that epidermal cell surface area is significantly greater in both adaxial and abaxial epidermal pavement cells of *Atham1,2,3* mutants relative to the wild type, while guard cells and trichomes are of comparable size in *Atham1,2,3* rosette leaves relative to the wild type (Fig. 3G). Comparison of adaxial and abaxial epidermal surface characteristics in *Atham1,2,3* mutants does not suggest leaf polarity defects.

Shoot phenotypes of *Atham1,2,3* mutants are most evident following the transition to reproductive growth, whereupon wild-type Arabidopsis plants typically exhibit secondary shoots emerging from axils of both rosette and inflorescence leaves (Fig. 3H). In mature *Atham1,2,3* mutant plants, secondary inflorescence stems rarely emerge from leaf axils of either rosette or primary inflorescence stem (Fig. 3H). Close examination of *Atham1,2,3* rosette axils by scanning electron microscopy reveals discrete populations of comparatively small cells, consistent with axillary meristem formation and subsequent axillary meristem arrest prior to the initiation of organogenesis of subtending stem or lateral organs (Fig. 3I). Higher magnification of rosette axils reveals stomatal pores in the axillary "meristem" epidermis, indicating differentiation of meristem cells following meristem arrest (Fig. 3J). Occasional rosette and inflorescence axils produce single, radially symmetrical organs (Fig. 3K).

While arrest of the primary vegetative meristem has not been observed to date in *Atham1,2,3* mutants, loss of indeterminacy occurs, with incomplete penetrance, in flower and primary inflorescence meristems. *Atham1,2,3* mutants are significantly delayed in the development of mature flowers relative to the wild type, consistent with delayed inflorescence development and/or delayed transition from vegetative to reproductive development (Fig. 4A). A subset of *Atham1,2,3* mutants exhibit loss of shoot indeterminacy following the transition to reproductive development, characterized by cessation of flower production and significant enlargement of the stem apex relative to the wild type (Fig. 4B; Supple-

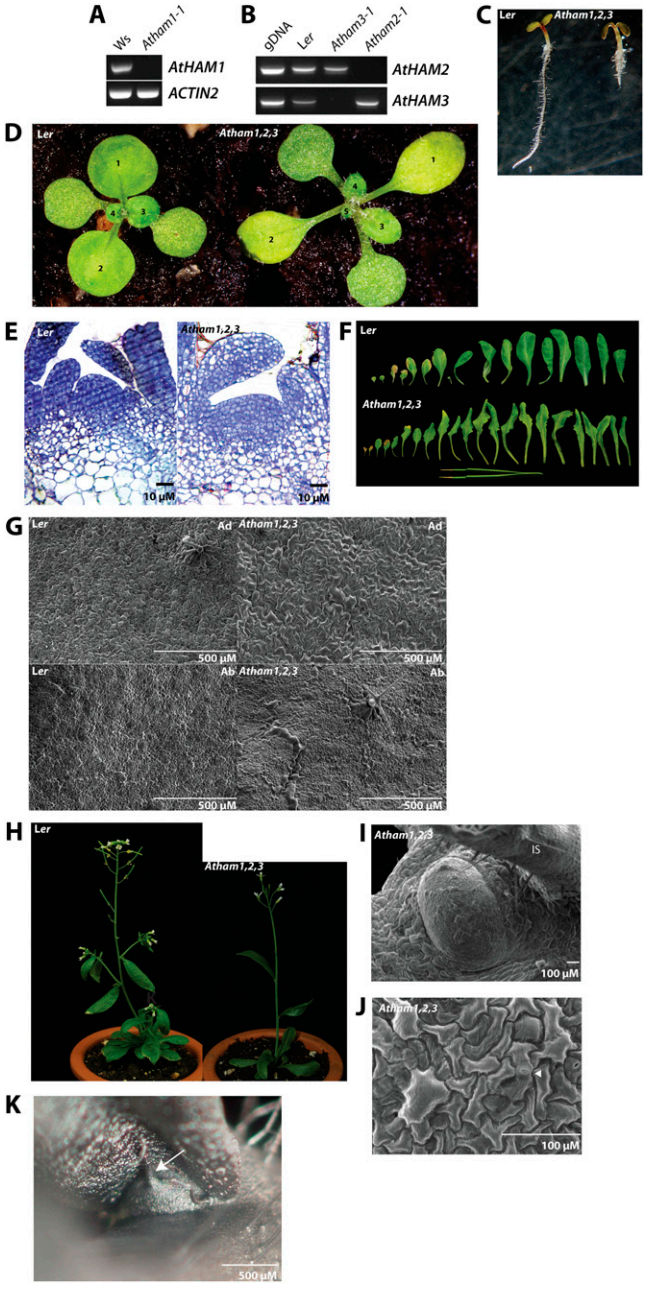

Figure 3. *Atham1,2,3* mutants exhibit arrest and differentiation of secondary meristems and altered structure and function of the primary shoot apical meristem. A, RT-PCR analysis of wild-type Wassilewskija (Ws) and a homozygous *Atham1-1* mutant with primers flanking the T-DNA insertion site (Supplemental Table S2). Primers designed to amplify *ACTIN2* cDNA were employed as a control for cDNA quality. B, RT-PCR analysis of wild-type L*er* and homozygous *Atham2-1* and *Atham3-1* mutants with primers flanking the Ds insertion sites (Supplemental Table S2). Amplification from genomic DNA (gDNA) is employed as a reference for product size and primer set efficacy. *AtHAM2* and *AtHAM3* primer sets serve as reciprocal controls for cDNA quality in L*er*, *Atham2-1*, and *Atham3-1* genotypes. C, L*er* and an *Atham1,2,3* mutant at 3 d postgermination on sterile medium. *Atham1,2,3* mutants exhibit elongation of the primary root, demonstrating the presence of a root meristem. The hypocotyl and cotyledons are evident in *Atham1,2,3* mutants and do not differ significantly from the wild type in appearance, although epinastic curvature of the cotyledons is common in *Atham1,2,3* mutants. D, L*er* and an *Atham1,2,3* mutant at 12 d postgermination. Postembryonic leaves are labeled (numbering of leaves 1 and 2 is arbitrary, as these two leaves arise roughly simultaneously). By emergence of the fourth leaf, deviations from wild-type phyllotaxis are apparent in many *Atham1,2,3* mutants. E, Longitudinal section through shoot apices of L*er* and an *Atham1,2,3* mutant at 12 d postgermination. *Atham1,2,3* mutants consistently exhibit broader and flatter primary shoot apical meristems relative to the wild type at 12 d postgermination, but significant differences in meristem size in *Atham1,2,3* mutants relative to the wild type are not evident. F, Set of fully expanded rosette leaves of L*er* and an *Atham1,2,3* mutant. Leaf 8 of L*er* is largely missing from this set. *Atham1,2,3* rosette leaves typically exhibit reduced laminar expansion relative to the wild type. G, Epidermal surfaces of fully expanded rosette leaves of L*er* and an *Atham1,2,3* mutant imaged by scanning electron microscopy. Increases in average epidermal cell surface area relative to the wild type are evident on both the adaxial (Ad) and abaxial (Ab) leaf surfaces of *Atham1,2,3* mutants. H, L*er* and *Atham1,2,3* mutant shoot phenotypes postflowering. Secondary shoots are typically in evidence emerging from axils of both the rosette and inflorescence at this stage in the wild type but are rarely observed in *Atham1,2,3* mutants. I and J, Surface of an arrested rosette axillary meristem of an *Atham1,2,3* mutant visualized by scanning electron microscopy. The main inflorescence stem (IS) is indicated for positional reference in I. The arrowhead in J indicates a fully differentiated stomata. K, Radially symmetrical multicellular structure, indicated with the arrow, emerging from an arrested axillary inflorescence meristem of an *Atham1,2,3* mutant, visualized by digital optical microscopy.

mental Video S1). Loss of indeterminacy in the inflorescence meristem is preceded by a gradual loss of meristem indeterminacy in flowers (Fig. 4, B and C), initially evident by flowers with reduced or missing inner whorls (F4 in Fig. 4C), progressing to flowers that fail to initiate lateral organs (F3 and F2 in Fig. 4C), and culminating in flowers that lack both pedicle and lateral organ development (F1 in Fig. 4C). As with the vegetative shoot meristem, functioning *Atham1,2,3* inflorescence meristems do not differ from the wild type with respect to meristem size, indicating that enlargement of the inflorescence apex in arrested *Atham1,2,3* inflorescences is likely a consequence of meristem differentiation rather than meristem enlargement preceding arrest (Fig. 4D). Further paralleling vegetative meristem abnormalities, *Atham1,2,3* inflorescences consistently exhibit aberrant phyllotaxis (Fig. 4E). However, functioning *Atham1,2,3* inflorescence meristems exhibit a suite of abnormalities not observed in vegetative apices, including vacuolization of meristem cells, supernumerary meristem cell layers, and an indistinct boundary between meristematic and differentiating tissue zones (Fig. 4D).

Atham1,2,3 cauline leaves typically exhibit epinastic curling, indicative of greater adaxial leaf surface area relative to abaxial leaf surface area (Fig. 4E). Analysis by scanning electron microscopy did not reveal appreciable differences in epidermal cell size between *Atham1,2,3* and the wild type on either the adaxial or abaxial cauline leaf surface (data not shown), indicating that curling results from an increase in cell number in

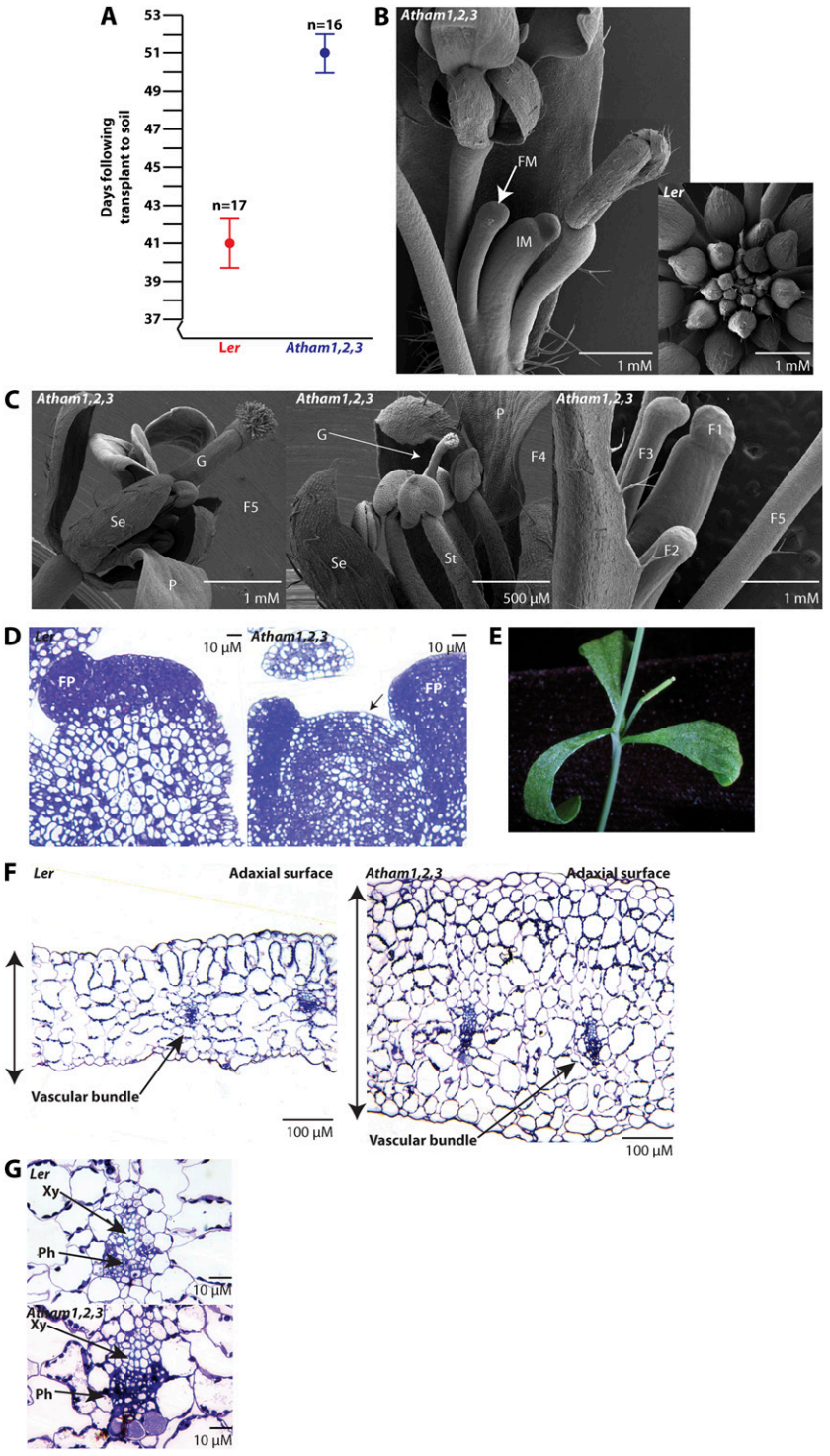

Figure 4. Inflorescence phenotypes of *Atham1,2,3* mutants. A, Time until flowering, assessed by petal emergence from the first flower, in L*er* and *Atham1,2,3* mutants. Error bars indicate 95% confidence interval of the mean. B, Inflorescence apices of an arrested *Atham1,2,3* mutant and L*er*, viewed with scanning electron microscopy. An arrested flower meristem (FM) is indicated to the left of the inflorescence meristem (IM). C, Progression in loss of indeterminacy in an *Atham1,2,3* inflorescence viewed with scanning electron microscopy. Floral organs are labeled as follows: gynoecium (G), stamen (St), petal (P), and sepal (Se). Flowers are labeled according to sequence of initiation (F1–F5). D, Median longitudinal sections through L*er* and *Atham1,2,3* mutant inflorescence apices stained with toluidine blue and visualized by bright-field microscopy. Flower primordia are indicated (FP). Wild-type meristem cells stain densely, indicating high concentrations of cytoplasm. The arrow indicates a vacuolated cell in the *Atham1,2,3* L1 meristem layer. Supernumerary meristem layers are evident in the *Atham1,2,3* meristem. E, Abnormal phyllotaxis and organ transformation in an *Atham1,2,3* mutant inflorescence. Three cauline leaves have arisen in close spatial and temporal proximity (compare with L*er* in Fig. 3H). A flower has developed in the axillary meristem of the right-most cauline leaf at the position normally occupied by a secondary inflorescence shoot. Epinastic curling of cauline leaves is typical of *Atham1,2,3* mutants. F, Cross sections through the cauline leaf lamina of L*er* and an *Atham1,2,3* mutant stained with toluidine blue and visualized by bright-field microscopy. Double-arrowed lines represent the approximate median thickness of adjacent cauline leaves. G, Vascular bundles of L*er* and *Atham1,2,3* cauline leaves. Xylem (Xy) is positioned adaxial to phloem (Ph) in *Atham1,2,3* cauline leaves.

the adaxial domain relative to the abaxial domain. Sectioning of L*er* and *Atham1,2,3* mutant cauline leaves reveals a significant increase in cell number along the adaxial/abaxial axis in *Atham1,2,3* mutants relative to the wild type (Fig. 4F). Wild-type patterning of vascular bundles demonstrates that adaxial/abaxial polarity is normal in *Atham1,2,3* mutant cauline leaves (Fig. 4G).

Atham1,2,3 Mutants Exhibit Abnormalities in Postembryonic Root Development, Including Reduced Rates of Cell Division in Root Meristems, Root Bifurcation, and Loss of Root Indeterminacy

Both *Petunia HAM* and *AtHAM* orthologs are expressed in root tissue, suggesting a role for HAM function in root development, although root abnor-

malities are not reported for *Petunia ham* mutants (Stuurman et al., 2002; Fig. 2). To determine if *Atham1,2,3* mutants are altered in root growth, we germinated seeds on sterile medium and monitored primary root elongation and overall root morphology. Alongside *Atham1,2,3* and wild-type L*er* seedlings, *shortroot2* (*shr2*) mutants were grown as a reference for root meristem arrest. *Atham1,2,3* mutants exhibit a significant reduction in elongation of the primary root relative to L*er*, comparable in degree to *shr2* mutants (Fig. 5, A and B). At 9 d following germination, primary root apices of *Atham1,2,3* mutants appear normal with respect to radial organization of the root meristem, but the size of *Atham1,2,3* root meristems is significantly reduced relative to the wild type in both longitudinal and radial axes (Fig. 5, C–E). A subset of *Atham1,2,3* root meristems exhibit starch staining in cells immediately adjacent to the quiescent center, at the position normally occupied by columella initials, indicating an incompletely penetrant phenotype of accelerated differentiation of the columella (data not shown). The primary root meristem is delineated in the longitudinal axis as the region extending from differentiating columella to the elongation zone, in which cell size remains relatively constant via continuing cell divisions. *Atham1,2,3* root meristems are significantly smaller in the longitudinal axis relative to the wild type, indicating either a reduced rate of cell division in the meristem or accelerated cellular differentiation and elongation (Fig. 5F). Reduction in root meristem diameter correlates with a reduced number of cells in radial tissue layers of *Atham1,2,3* roots relative to the wild type (Fig. 5E). By 10 d following germination, radial meristem organization and the quiescent center are no longer discernible in a subset of *Atham1,2,3* mutant root apices, indicating loss of root indeterminacy (Fig. 5G). Two of 33 *Atham1,2,3* mutant roots examined exhibited root bifurcation, with two root meristems located adjacent to one another at a single root apex (root fasciation; Fig. 5H).

Reduced primary root elongation in *Atham1,2,3* mutants prior to loss of root indeterminacy could be reasoned a priori to result from (1) a reduction in the magnitude of root cell elongation or (2) a reduced rate of cell division in the root meristem. To determine if *Atham1,2,3* mutants exhibit reduced root cell elongation, we measured the length of atrichoblast cells within the zone of root hair elongation from L*er* and *Atham1,2,3* mutants. Atrichoblasts of *Atham1,2,3* are not significantly different in length from atrichoblasts of wild-type seedlings, demonstrating that the reduction in primary root length in *Atham1,2,3* mutants is not attributable to reduced root cell elongation (Supplemental Fig. S3). We conclude that reduced root elongation in *Atham1,2,3* mutants is the result of decreased rates of cell division in the root meristem.

Regulation of root meristem identity is the function of the quiescent center, and maintenance of the root quiescent center requires the generation of an auxin maximum at the root apex (Blilou et al., 2005; Grieneisen et al., 2007). Loss of root indeterminacy in *Atham1,2,3* mutants could result from the inability to generate a wild-type auxin maximum at their root apices. If this were the case, we would predict that functioning *Atham1,2,3* root apices may exhibit auxin maximum defects prior to full meristem arrest. To test this hypothesis, we visualized relative auxin levels in the primary root apices of Columbia and *Atham1,2,3* mutants using the DR5::GUS auxin reporter system at 6 d following germination, when reduction in primary root elongation is readily discernible in *Atham1,2,3* mutants (Ulmasov et al., 1997). *Atham1,2,3* mutants exhibit root apex auxin maxima that are comparable to the wild type in spatial expression and intensity, consistent with *Atham1,2,3* mutant root phenotypes not being principally a consequence of altered auxin transport at the root apex (Fig. 5I).

Atham1,2,3 Mutant Root Hairs Exhibit Elevated Levels of Branching and Transient Loss of Anisotropic Tip Growth

In examining *Atham1,2,3* roots, we observed a significant number of branched root hairs (Fig. 6). Fifty-two percent of *Atham1,2,3* root hairs are branched (n = 10, 2× SEM = 11%), while no branched root hairs were detected in the L*er* roots examined. Root hair branches of *Atham1,2,3* mutants emerge from swollen sections of the main root hair shaft, consistent with a transient reversion from anisotropic tip growth to isotropic growth coincident with or immediately preceding the initiation of a second site of tip growth. Swellings in the root hair shaft without associated branches are also common on *Atham1,2,3* roots but are rarely noted on L*er* roots. The frequency of root hair branching and root hair swelling in *Atham1,2,3* mutants is not continuous along the length of the primary root but occurs in patches of highly elevated branching, interrupted by regions of root hairs exhibiting wild-type anisotropic growth.

AtHAM4 Genetically Interacts with *AtHAM1* and *AtHAM2* in Promoting Shoot Indeterminacy

The probable lack of MIR regulation in *AtHAM4*, coupled with the degree of evolutionary divergence between the HAM I and HAM II lineages, suggest that *AtHAM4* may have evolved novel functions and patterns of expression and may exhibit limited functional overlap with *AtHAM1*, *AtHAM2*, and *AtHAM3* (Fig. 1, A and B). To determine if and to what extent *AtHAM4* exhibits functional redundancy with Arabidopsis *HAM* orthologs, we obtained a knockout allele of *AtHAM4* (Fig. 7A; Supplemental Fig. S2) and undertook to generate multiple mutant combinations between *Atham1*, *Atham2*, *Atham3*, and *Atham4*. *Atham4* mutants exhibit no striking abnormalities in shoot development, although they are consistently of smaller overall stature relative to the wild type (Fig. 7B). *Atham1,4* double mutants similarly exhibit no striking shoot abnormalities (Fig. 7C). However, *Atham1,4; Atham2*/+ mutants exhibit a range of variably penetrant phenotypes, from a loss of primary

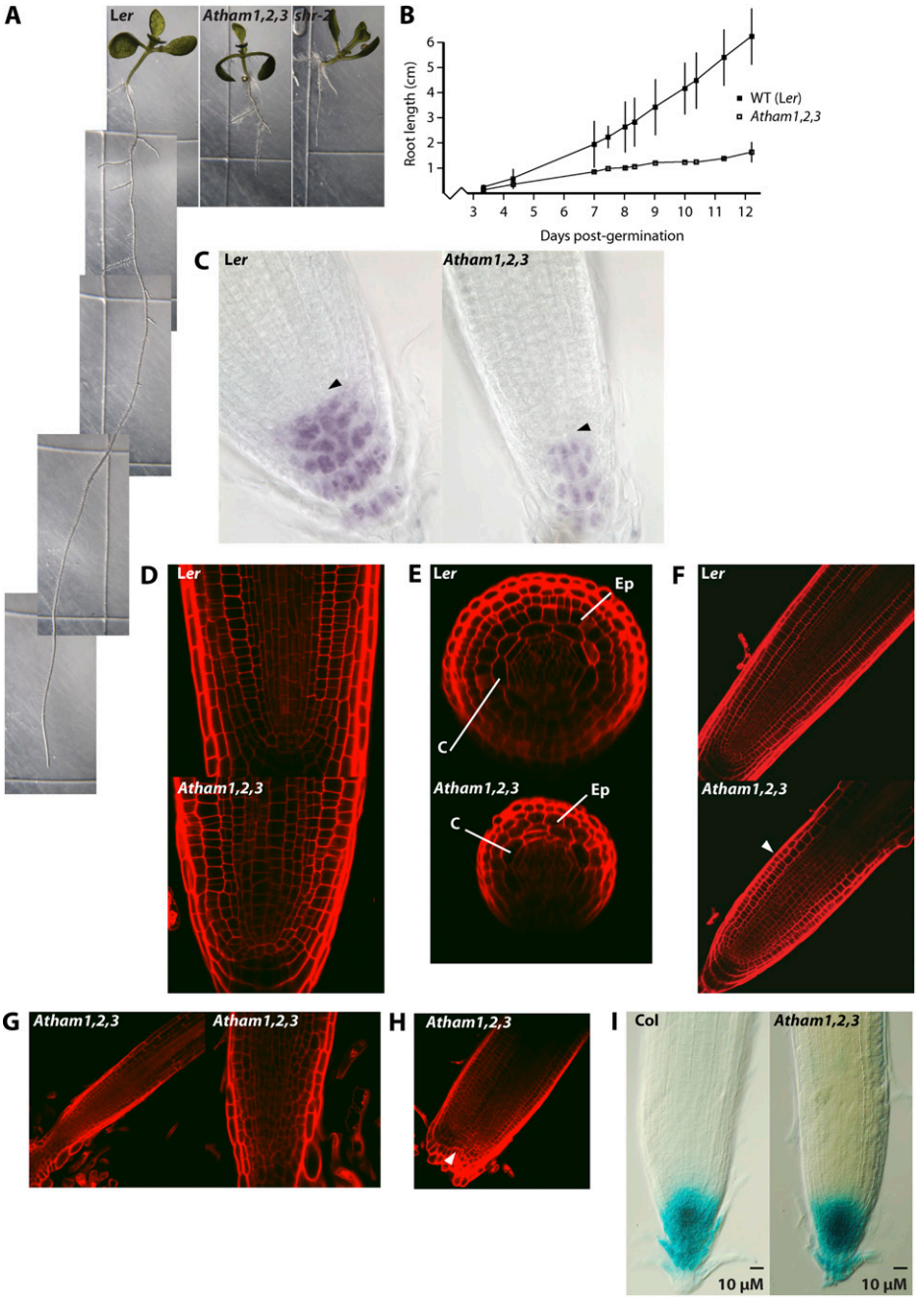

Figure 5. Root phenotypes of *Atham1,2,3* mutants. A, L*er*, *Atham1,2,3*, and *shr2* plants grown for 12 d following germination on sterile medium. *Atham1,2,3* mutants exhibit comparable reductions in primary root length relative to the wild type as *shr2* mutants. B, Primary root growth rate of L*er* and *Atham1,2,3* mutants grown for 12 d following germination on sterile medium. Error bars indicate 2× SEM. WT, Wild type. C, Lugol-stained roots of L*er* and an *Atham1,2,3* mutant at 9 d following germination viewed by bright-field microscopy. Purple staining indicates starch granules in differentiated columella cells. The position of the quiescent center is indicated with the arrowheads. The reduction in primary root diameter in *Atham1,2,3* mutants relative to the wild type is evident. D to H, Optical cross sections through primary root apices of L*er* and *Atham1,2,3* mutants visualized by confocal microscopy. D, F, G, and H show longitudinal cross sections through the root meristems of L*er* and *Atham1,2,3* mutants at 9 d following germination. The boundary between the root meristem and elongation zone is indicated in F, with the white arrowhead in the *Atham1,2,3* panel, and is outside the frame of the L*er* panel. E, Radial cross sections of L*er* and *Atham1,2,3* mutant meristematic zones at 9 d following germination. Epidermis (Ep) and cortex (C) are indicated. G, An *Atham1,2,3* mutant at 10 d following germination shows loss of meristem indeterminacy. H, Longitudinal section through the root apex of an *Atham1,2,3* mutant exhibiting root meristem bifurcation. I, Root apices of Columbia (Col) and *Atham1,2,3* mutant roots expressing the pDR5::GUS auxin reporter construct stained with 5-bromo-4-chloro-3-indolyl-β-D-GlcUA and visualized by differential interference contrast microscopy. The intensity of blue staining is proportional to free auxin concentration. Shown are primary roots at 6 d following germination.

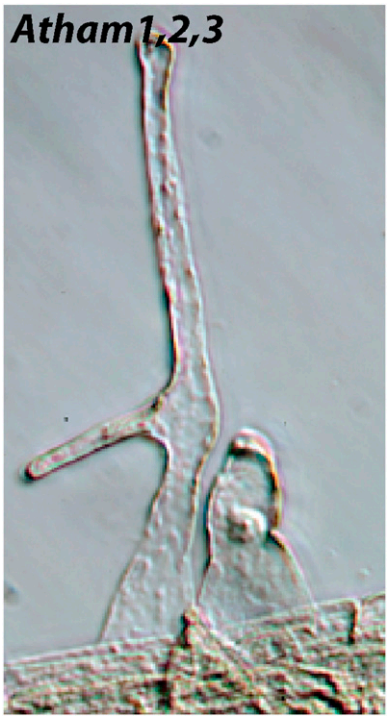

Figure 6. *Atham1,2,3* mutant root hairs exhibit elevated rates of branching and swelling. Two root hairs from the zone of root hair elongation on the primary root of an *Atham1,2,3* mutant are visualized by differential interference contrast microscopy. The root hair on the left exhibits branching morphology typical of *Atham1,2,3* root hairs, with the branch point site associated with transient swelling of the root hair shaft. The root hair on the right exhibits transient swelling of the basal root hair shaft, an anisotropic growth defect frequently observed among *Atham1,2,3* mutant root hairs. [See online article for color version of this figure.]

inflorescence shoot dominance to arrest and differentiation of the inflorescence meristem prior to flower initiation (Fig. 7C). *Atham1,4; Atham2*/+ mutants frequently exhibit a secondary meristem phenotype characterized by the production of a novel organ consisting of a leaf subtended by a stem similar in size to a flower pedicle (Fig. 7D), a structure observed less frequently in *Atham1,2,3* mutants (data not shown). *Atham1,2,4* mutants consistently exhibit an absence of secondary rosette stems and arrest and differentiation of flower and primary inflorescence meristems, similar to the most extreme phenotypes of *Atham1,2,3* mutants (Fig. 7, E and F). Collectively, these results demonstrate significant functional redundancy between *AtHAM4* and *AtHAM1* and *AtHAM2* in promoting shoot indeterminacy.

DISCUSSION

Flowering Plant *HAM* Genes Are Likely to Possess Both Core Ancestral and Angiosperm-Specific Functions

The presence of *HAM* homologs in the genomes of the basal plants *Physcomitrella* and *Selaginella*, and conservation of the domain structure and MIR-binding sequence among distantly related HAM proteins, suggest that aspects of flowering plant HAM function may be derived from the common ancestor of bryophytes and vascular plants and that ancestral functions may be shared among extant flowering and basal plants. Determining what the core ancestral HAM function is must await genetic ablation of *HAM* homologs in *Physcomitrella* and *Selaginella* and/or the complementation of flowering plant *ham* mutants with basal plant *HAM* homologs.

The dramatic expansion in *HAM* homolog diversity in flowering plants strongly suggests the evolution of novel *HAM* functions or functional *HAM* subspecialization in angiosperms, while elevated rates of evolution in flowering plant *HAM* homologs indicate a refinement of HAM function in response to novel selective pressures. Supporting the model of acquisition of novel functions by at least a subset of flowering plant *HAM* genes is the probable loss of MIR-mediated regulation on multiple, independent occasions, suggesting a strong selective pressure in flowering plants that favored the expansion of *HAM* expression. Modification of expression domains may be a major evolutionary force preceding the acquisition of novel functions (Matsuno et al., 2009), and modification to MIR-binding sequences is proposed to be an evolutionarily significant source of variation generation (Chen and Rajewsky, 2007; Ehrenreich and Purugganan, 2008). Observed sequence divergences in *HAM* MIR-binding sequences are likely to reflect an absence of MIR-mediated posttranscriptional regulation, although binding of MIRs to their target sequences may be tolerant of low levels of internal and 5′ nucleotide mismatch, and the possibility of novel miRs in the genomes of many of the species surveyed cannot be discounted (Mallory et al., 2004). The ancestral MIR-binding sequence is perfectly conserved in all eudicot members of the HAM II clade for which complete sequences are available, indicating a function common to all eudicot HAM II proteins that exerts strong selective pressure to conserve the ancestral MIR-binding sequence and limit *HAM* expression. Loss of MIR regulation may be preceded by the disruption of some component of HAM function that removes this constraint, or, alternatively, the loss of MIR regulation may occur in *HAM* paralogs that evolve nonoverlapping patterns of expression with their ancestral miR regulators.

All Four Arabidopsis *HAM* Homologs Promote Shoot Indeterminacy

Atham1,2,4 mutants exhibit stronger shoot meristem arrest phenotypes than *Atham1,2,3* mutants, demonstrating that *AtHAM4* contributes significantly to the maintenance of shoot indeterminacy and functions redundantly with *AtHAM1* and *AtHAM2*. These results suggest that some degree of HAM-mediated indeterminacy may be retained in triple mutant com-

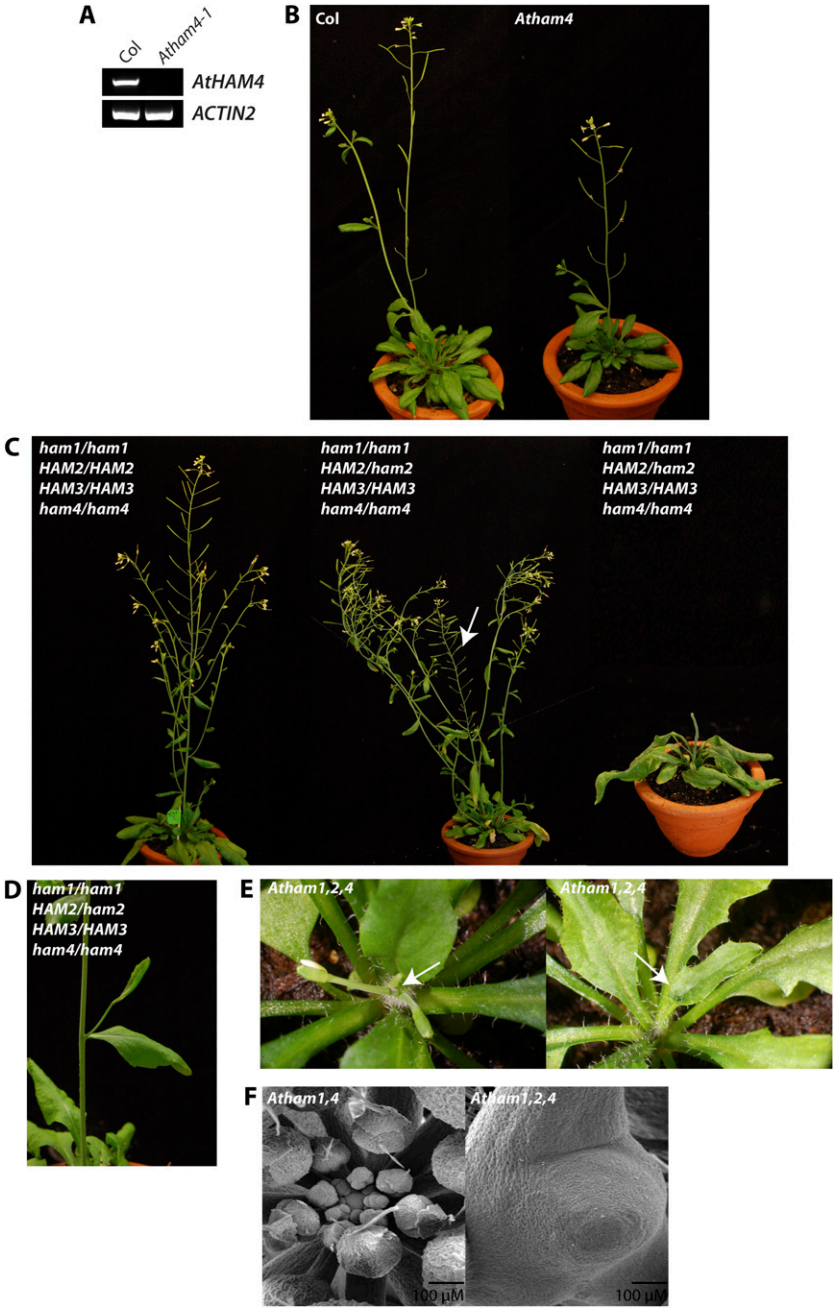

Figure 7. Shoot phenotypes of *Atham4*, *Atham1,4; Atham2/+*, and *Atham1,2,4* mutants. A, RT-PCR analysis of wild-type Columbia (Col) and a homozygous *Atham4-1* mutant with primers flanking the T-DNA insertion site (Supplemental Table S2). Primers designed to amplify *ACTIN2* cDNA were employed as a control for cDNA quality. B, Columbia and *Atham4* mutant shoot phenotypes postflowering. *Atham4* mutants consistently exhibit reduced stature relative to the wild type but do not otherwise exhibit obvious abnormal phenotypes. C, Shoot phenotypes of *Atham1,4* mutant and *Atham1,4; Atham2/+* genotypes. *Atham1,4* mutants do not exhibit obvious shoot phenotype abnormalities. Shoot phenotypes of *Atham1,4; Atham2/+* plants are highly variable. The middle plant is an *Atham1,4; Atham2/+* plant exhibiting reduced dominance of the primary inflorescence stem, indicated by the arrow, relative to wild-type plants. The right-most plant is an *Atham1,4; Atham2/+* plant exhibiting an absence of secondary growth in the rosette and arrest of the primary inflorescence meristem prior to the initiation of flowers. D, Novel organ formation in the inflorescence axil of an *Atham1,4; Atham2/+* plant. At the position normally occupied by a secondary inflorescence stem, a leaf subtended by a short stem resembling a flower pedicle is evident. The orientation of the adaxial leaf surface is away from the adjoining inflorescence stem. E, Shoot phenotypes of *Atham1,2,4* mutants. The left-hand panel shows an *Atham1,2,4* mutant with arrested flower and inflorescence meristems. The inflorescence meristem is indicated by the arrow. No secondary stems are in evidence emerging from the rosette. The right-hand panel shows an *Atham1,2,4* mutant inflorescence terminating in a single "trumpet-leaf" cauline leaf. F, Inflorescence apices of *Atham1,4* and *Atham1,2,4* mutants visualized by scanning electron microscopy.

binations and that the generation and analysis of *Atham1,2,3,4* quadruple mutants will be required to define the full contribution of *AtHAM*s to the maintenance of indeterminacy. The variable penetrance of meristem-arrest phenotypes in *Atham1,2,3* and *Atham1,4; Atham2/+* mutants is consistent with the retention of HAM function, the degree of HAM function retained being stochastic in the loss-of-function backgrounds examined. Similarly, the variably penetrant phenotype of *Petunia ham*, coupled with the observation that eudicots with completed genomes all possess at least two *HAM* homologs, suggest that at minimum a second *HAM* homolog resides in the *Petunia* genome, which functions redundantly with the originally identified *HAM* gene.

Do HAM Proteins Function Non Cell Autonomously?

Petunia HAM is inferred to promote shoot indeterminacy by a non-cell-autonomous mechanism on the bases of (1) the absence of detectable *HAM* expression in much of the shoot meristem and (2) the complementation of the *ham* phenotype by L3-restricted *HAM* expression (Stuurman et al., 2002). Non-cell-autonomous functioning is well established for the related GRAS protein SHR, and the VHIID and PYFRE do-

mains, conserved among SHR and HAM proteins, are required for intracellular movement of SHR (Nakajima et al., 2001; Gallagher and Benfey, 2009). *AtHAM1* expression in Arabidopsis shoot apices overlaps significantly with the reported expression of *Petunia HAM* but clearly extends farther toward the Arabidopsis meristem apex than is reported for *Petunia HAM*, overlapping with expression domains of meristem autonomous regulators of indeterminacy such as *WUSCHEL* and *SHOOTMERISTEMLESS* (Long et al., 1996; Mayer et al., 1998). In the root, the potential for non-cell-autonomous promotion of root indeterminacy by *AtHAM*s appears low, as *AtHAM1*, *AtHAM2*, and *AtHAM3* are expressed nearly constitutively in the root. In situ hybridization may fail to detect transcripts expressed at very low, yet potentially functional, levels; therefore, inferences that depend upon in situ hybridization to establish an absence of expression must be regarded cautiously. The data presented in this study do not directly inform our understanding of whether *AtHAM*s function cell autonomously or non cell autonomously. However, the detailed characterization of *Atham* loss-of-function phenotypes described here provides a foundation for developing future experiments to directly test the model of *HAM* functioning via a non-cell-autonomous pathway.

What Is the Cellular Function of HAM Proteins?

The highly pleiotropic phenotype of *Atham1,2,3* mutants, including expanded anticlinal cell divisions in developing cauline leaves, reduced levels of cell division in root meristems, and root hair branching, coupled with the broad expression patterns of *AtHAM1*, *AtHAM2*, and *AtHAM3* in shoot and root tissue demonstrate that HAM function is not limited to promoting organ indeterminacy and may inform the development of models for HAM function at the cellular level. The diverse suite of *ham* loss-of-function phenotypes may reflect HAM function in the transmission of a specific stimulus that regulates a broad spectrum of cellular and developmental processes, such as a hormone. In this context, it is notable that within the GRAS protein family, HAM proteins are most closely related to DELLA proteins, transcriptional regulators whose function and stability are mediated by gibberellins (Harberd et al., 2009; E.M. Engstrom, unpublished data). Alternatively, HAM proteins may regulate a specific cellular function that has broad developmental consequences, such as cell cycle progression. Canonical cell cycle regulatory proteins regulate stem cell identity, indeterminacy, and organ patterning in roots, suggesting that regulation of indeterminacy may occur at least in part through the regulation of cell cycle progression (Wildwater et al., 2005; Sozzani et al., 2010). Moreover, the GRAS proteins SCARECROW and SHR are not only similarly required for the maintenance of root indeterminacy (Di Laurenzio et al., 1996; Helariutta et al., 2000; Sabatini et al., 2003) but also regulate the transcription of a set of cell cycle regulatory proteins, including RETINOBLASTOMA RELATED, D cyclins, and E2F factors in developing leaves and D cyclins and cyclin-dependent kinases in the root (Dhondt et al., 2010; Sozzani et al., 2010). Regulation of cell cycle progression is a plausible candidate for a cell-level HAM function that could explain much of *ham* loss-of-function phenotypes, and the expression of cell cycle regulators in *Atham* backgrounds warrants examination.

ham1,2,3 Mutant Phenotypes Overlap Considerably with *fasciata1* and *fasciata2* Phenotypes

FASCIATA1 (*FAS1*) and *FAS2* encode components of the chromatin assembly factor 1, which regulates nucleosome assembly, chromatin silencing, and homologous recombination (Endo et al., 2006; Kirik et al., 2006; Ono et al., 2006; Schönrock et al., 2006). "Fasciation" refers to phenotypes attributable to multifurcating shoot apices, resulting in supernumerary, fused lateral organs and flattened, ridged stems (Worsdell, 1905). In addition to exhibiting fasciation phenotypes, *fas1* and *fas2* exhibit highly pleiotropic shoot and root phenotypes, aspects of which significantly parallel *Atham1,2,3* mutant phenotypes, including broadened and relatively flat shoot apical meristems, ectopic vacuolization in the meristem, abnormal phyllotaxis, enlarged epidermal cell size, impaired root growth, and occasional meristem arrest in *fas2* mutants (Reinholz, 1966; Ottoline Leyser and Furner, 1992; Kaya et al., 2001; Exner et al., 2006). Further paralleling *AtHAM* loss-of-function phenotypes, *fas1* and *fas2* mutant phenotypes are restricted to postembryonic development and exhibit enhanced branching of trichomes, similar to the enhanced branching of root hairs exhibited by *Atham1,2,3* mutants (Kaya et al., 2001; Exner et al., 2006). Fasciation of the root, as is observed in *Atham1,2,3* mutants, has not been reported to date in *fas1* or *fas2* mutants that we are aware of. As DNA modification enzymes, FAS1 and FAS2 are plausible candidates for physical interactions with HAM transcription factors.

MATERIALS AND METHODS

Phylogenetic Analysis

Multiple sequence alignments were generated with the ClustalW program (Larkin et al., 2007) using Geneious Pro 4.6.4 software, employing a GONNET cost matrix, a gap opening penalty of 35, and a gap extension penalty of 0.75. Resulting alignments were then refined by eye using the Geneious Pro 4.6.4 software. GRAS proteins exhibit substantial sequence divergence in their N-terminal regions, precluding accurate alignment for roughly the N-terminal-most one-third of GRAS proteins. An aligned region corresponding to amino acids 358 to 721 of the *Petunia hybrida* HAM protein was extracted from the complete protein alignments and manually refined prior to phylogenetic analyses. Final protein alignments are available upon request from the corresponding author.

Phylogenetic analysis by the Bayesian inference method was performed with the MrBayes program (Huelsenbeck and Ronquist, 2001) via Geneious Pro 4.6.4 software, employing a Poisson amino acid rate matrix and a gamma rate variation. A total of 120,000 generations were generated, and every 1,000th tree was saved. Four independent chains were run with a temperature of 0.1, and the initial 30,000 trees were discarded as burn in. The analysis was

run long enough to attain a SD of split frequencies of less than 0.02. A SD of split frequencies of less than 0.02 was obtained at generation 69,000 and remained relatively stable thereafter, indicating that additional generations are unlikely to improve the accuracy of the tree with these parameters.

Plant Material

Arabidopsis (*Arabidopsis thaliana*) *Atham1-1* seed was obtained from the INRA. The *Atham1-1* insertion (FLAG_239F03; Samson et al., 2002) is localized 5′ and in close proximity to position +742 relative to the translational start site in the Wassilewskija ecotype. Efforts to more precisely map the *Atham1-1* insertion site have not been successful due to an inability to amplify fragments containing portions of the T-DNA. The wild-type allele of *AtHAM1* was identified by PCR (Supplemental Table S3). *Atham2-1* and *Atham3-1* seed was provided by Dr. Venkatesan Sundaresan. The *Atham2-1* insertion (SGT11982) is localized to position +1,303 relative to the translational start site in the L*er* ecotype (Sundaresan et al., 1995). The *Atham3-1* insertion (SGT13186) is localized to position +920 relative to the translational start site in the L*er* ecotype (Sundaresan et al., 1995). Wild-type and Ds insertion alleles of *AtHAM2* and *AtHAM3* were identified by PCR (Supplemental Table S3). Insertion sites of *Atham2-1* and *Atham3-1* alleles were identified by sequencing PCR-amplified products derived from the Forward and Ds30 primer sets (Supplemental Table S3). *Atham4-1* seed was obtained from the Arabidopsis Biological Resource Center. The *Atham4-1* insertion (SALK_110871; Alonso et al., 2003) is localized to position +1,046 relative to the translational start site in the Columbia ecotype. *shr2* seed (Helariutta et al., 2000) was obtained from the Arabidopsis Biological Resource Center. *Atham2-1*, *Atham3-1*, and *Atham1,2,3* mutant lines have been deposited at the Arabidopsis Biological Resource Center.

Growth Conditions and Measurements

Soil-grown plants were maintained at 20°C with a 16-h daylength under cool-white fluorescent bulbs (8.3 ± 0.93 kilolux). For analysis of root phenotypes, seeds were germinated and maintained on vertically oriented plates containing 0.5× Murashige and Skoog salts, 1% Suc, and 0.7% phytagel (Sigma-Aldrich). For measurements of root length, photographs of entire seedlings were taken at intervals through a Zeiss Discovery V12 stereomicroscope equipped with a 0.63× objective and coupled to a Nikon D50 SLR digital camera. For measurements of root cell length, seedlings grown on vertical plates were removed, placed in a bath of 0.5× Murashige and Skoog salts on a coverslip, and sections of the zone of root hair elongation were photographed through a Zeiss Axiovert 40 CFL microscope equipped with a long-distance 40× Apoplan objective (numerical aperture [N.A.] 1.0) and coupled to a Nikon D50 SLR digital camera. Root and root cell lengths were measured using the Ruler Tool of Photoshop (Adobe).

Flowering Time Assay

Seeds of L*er* and *Atham1,2,3* mutant genotypes were surface sterilized, germinated on 0.5× Murashige and Skoog salts and 0.6% phytagel (Sigma-Aldrich), and maintained at 18°C with a 16-h daylength for 6 d. Seedlings for which the cotyledons had expanded and the first two postembryonic leaves were clearly visible were transplanted to soil (day 0) and maintained at 20°C with a 16-h daylength under cool-white fluorescent bulbs. Plants were examined daily for an additional 53 d, and the time, measured in days, at which petals emerged from the first flower was recorded for each plant.

Histology

For tissue sectioning in plastic resin, tissue was placed in 2% paraformaldehyde and 2.5% glutaraldehyde in 0.025 M phosphate buffer (sodium phosphate, pH 7.4), vacuum was applied for 30 min, and tissue was fixed overnight at 4°C. Tissue was then rinsed twice with 0.025 M phosphate buffer, postfixed with 1% osmium tetroxide in 0.025 M phosphate buffer for 30 min, and moved through an increasing acetone series (20% increments), each increment lasting a minimum of 1 h and ending with two exchanges of 100% acetone. Tissue was then infiltrated with 812 epoxy resin by sequential transfer through a series of increasing resin concentrations in acetone (1:2, 1:1, and 2:1, 100%) and embedded in 812 resin for 3 d at 70°C in molds. Sections of 900 nm were cut with a diamond knife on a MT6000-XL ultramicrotome (RMC), and individual sections were mounted on glass slides. Slides were placed on a 50°C hot plate for 1 min, and a drop of 1% toluidine blue/1% sodium borate was applied to each section and allowed to stain for 1 min. Slides were then rinsed with distilled water and examined and photographed using bright-field microscopy with a Zeiss Axiovert 40 CFL microscope equipped with a long-distance 40× Apoplan objective (N.A. 1.0) and coupled to a Nikon D50 SLR digital camera.

For scanning electron microscopy, tissue was placed in 1.2% glutaraldehyde in 0.025 M phosphate buffer (sodium phosphate, pH 6.8), vacuum was applied for 10 min, and tissue was fixed overnight at 4°C. Tissue was then rinsed twice with 0.025 M phosphate buffer for 1 h, postfixed with 0.5% osmium tetroxide in 0.025 M phosphate buffer for 24 h at room temperature, and moved through an increasing ethanol series (20% increments), each increment lasting a minimum of 1 h and ending with two exchanges of 100% ethanol. Ethanol was removed by critical point drying with a critical point drier (SAMDRI), and tissue was mounted to stubs with double-sided adhesive tape and sputter coated with gold-palladium alloy using a Hummer Sputtering System (Anatech). Samples were examined with either a Hitachi 4700 or a Hitachi S-570 scanning electron microscope.

Confocal Microscopy

Roots of plants at 5 to 15 d after germination were stained for 2 min with 10 μM propidium iodide and imaged by laser scanning confocal microscopy using a Zeiss LSM 510 microscope. Transverse sections were taken at the middle of the meristematic zone.

Starch Staining

Roots of plants at 5 to 8 d after germination were fixed in ethanol:acetic acid (3:1, v/v) for 3 min, stained with Lugol solution (Sigma) for 1 min, mounted in chloral hydrate, and imaged using a Leica DM 5000B compound microscope.

pDR5::GUS Expression Analysis

Seeds of pDR5::GUS in Columbia and *Atham1,2,3* genotypes were sterilized and germinated on vertically oriented plates containing 0.5× Murashige and Skoog salts, 1% Suc, and 0.7% phytagel (Sigma-Aldrich). Roots were excised from seedlings 6 d after germination and immersed in ice-cold 90% acetone for 20 min, followed by three rinses in GUS working solution (33 mM sodium phosphate buffer, pH 7.0, 1.7 mM potassium ferricyanide, 1.7 mM potassium ferrocyanide, 1 mM EDTA, pH 8.0, and 1% Triton X-100) for 20 min. Roots were then stained in GUS staining solution (GUS working solution with 2 mM 5-bromo-4-chloro-3-indolyl-β-D-GlcUA) for 3 h at 37°C in darkness. Staining solution was removed, and roots were cleared with 70% chloral hydrate, 10% glycerol at 4°C for 48 h. Roots were examined and photographed using differential interference contrast microscopy with a Zeiss Axiovert 40 CFL microscope equipped with a long-distance 40× Apoplan objective (N.A. 1.0) coupled to a Nikon D50 SLR digital camera.

RT-PCR

Total RNA was extracted from tissues of 12-d-old seedlings with the RNeasy kit (Qiagen). RNA was DNase treated using the Turbo DNA-free kit (Ambion). Total cDNA was then prepared from approximately 1.6 μg of DNA-free total RNA using the SuperScript III kit (Invitrogen) with random hexamers according to the manufacturer's protocol. *AtHAM1* cDNA was amplified with the *AtHAM1* T-DNA flanking primer set, *AtHAM2* cDNA was amplified with the *AtHAM2* 5′ of Ds insertion primer set, and *AtHAM3* cDNA was amplified with the *AtHAM2* 5′ of Ds insertion primer set (Supplemental Table S2). *AtHAM4* cDNA was amplified with the *AtHAM4* T-DNA flanking primer set (Supplemental Table S3). All primer pairs amplify a segment of their respective target cDNAs containing their respective MIR-binding sites and consequently are selective to intact cDNA relative to MIR degradation products.

In Situ Hybridization

In situ hybridizations were performed following a modified protocol of Vielle-Calzada et al. (1999). A detailed protocol is available from the corresponding author upon request.

Supplemental Data

The following materials are available in the online version of this article.

Supplemental Figure S1. Expression domains of Arabidopsis *HAM* orthologs in both shoot meristem and root tissues.

Supplemental Figure S2. Loss-of-function alleles of Arabidopsis homologs of *Petunia HAM*.

Supplemental Figure S3. Reduction in primary root elongation in *Atham1,2,3* mutants results from reduced rates of cell division in the root meristem.

Supplemental Table S1. DELLA and HAM subfamily proteins used for phylogenetic analysis in Figure 1.

Supplemental Table S2. Oligonucleotide primer sequences used for RT-PCR amplification of *AtHAM* gene fragments.

Supplemental Table S3. Oligonucleotide primer sequences used for PCR genotyping of *Atham* insertional alleles.

Supplemental Video S1. Arrested inflorescence and flower meristems of an *Atham1,2,3* mutant visualized by digital optical microscopy.

ACKNOWLEDGMENTS

We thank Venkatesan Sundaresan and Pat Hogan for providing us with Ds insertion alleles of *AtHAM2* and *AtHAM3* and the Genetic Resources Team of the Institut Jean-Pierre Bourgin for sending us the Flag_239FO3 allele of *AtHAM1*. We thank Tom Guilfoyle for seeds of DR5::GUS in the Columbia background. Carla Wood, Tyler McEarcharn, and Johanna Smyth contributed to the construction of the *Atham1,2,3* mutant. Matthew Chang contributed to the construction and characterization of the *Atham1,2,4* mutant. Scanning electron microscopy and digital optical microscopy were performed at the Applied Research Center of the College of William and Mary with technical assistance from Brandt Robertson and Olga Trofimova. We thank Diane Shakes for critical reading of the manuscript, two anonymous reviewers for helpful comments on the manuscript, and Philip Benfey for valuable assistance with this project.

Received November 4, 2010; accepted December 7, 2010; published December 20, 2010.

LITERATURE CITED

Alonso JM, Stepanova AN, Leisse TJ, Kim CJ, Chen H, Shinn P, Stevenson DK, Zimmerman J, Barajas P, Cheuk R, et al (2003) Genome-wide insertional mutagenesis of Arabidopsis thaliana. Science **301:** 653–657

Axtell MJ, Snyder JA, Bartel DP (2007) Common functions for diverse small RNAs of land plants. Plant Cell **19:** 1750–1769

Baulcombe D (2004) RNA silencing in plants. Nature **431:** 356–363

Birnbaum K, Shasha DE, Wang JY, Jung JW, Lambert GM, Galbraith DW, Benfey PN (2003) A gene expression map of the Arabidopsis root. Science **302:** 1956–1960

Blilou I, Xu J, Wildwater M, Willemsen V, Paponov I, Friml J, Heidstra R, Aida M, Palme K, Scheres B (2005) The PIN auxin efflux facilitator network controls growth and patterning in Arabidopsis roots. Nature **433:** 39–44

Bolle C (2004) The role of GRAS proteins in plant signal transduction and development. Planta **218:** 683–692

Brady SM, Orlando DA, Lee JY, Wang JY, Koch J, Dinneny JR, Mace D, Ohler U, Benfey PN (2007) A high-resolution root spatiotemporal map reveals dominant expression patterns. Science **318:** 801–806

Brodersen P, Voinnet O (2006) The diversity of RNA silencing pathways in plants. Trends Genet **22:** 268–280

Carlsbecker A, Lee JY, Roberts CJ, Dettmer J, Lehesranta S, Zhou J, Lindgren O, Moreno-Risueno MA, Vatén A, Thitamadee S, et al (2010) Cell signalling by microRNA165/6 directs gene dose-dependent root cell fate. Nature **465:** 316–321

Chen K, Rajewsky N (2007) The evolution of gene regulation by transcription factors and microRNAs. Nat Rev Genet **8:** 93–103

Dhondt S, Coppens F, De Winter F, Swarup K, Merks RMH, Inzé D, Bennett MJ, Beemster GTS (2010) SHORT-ROOT and SCARECROW regulate leaf growth in Arabidopsis by stimulating S-phase progression of the cell cycle. Plant Physiol **154:** 1183–1195

Di Laurenzio L, Wysocka-Diller J, Malamy JE, Pysh L, Helariutta Y, Freshour G, Hahn MG, Feldmann KA, Benfey PN (1996) The SCARECROW gene regulates an asymmetric cell division that is essential for generating the radial organization of the Arabidopsis root. Cell **86:** 423–433

Dinneny JR, Benfey PN (2008) Plant stem cell niches: standing the test of time. Cell **132:** 553–557

Ehrenreich IM, Purugganan MD (2008) Sequence variation of microRNAs and their binding sites in Arabidopsis. Plant Physiol **146:** 1974–1982

Endo M, Ishikawa Y, Osakabe K, Nakayama S, Kaya H, Araki T, Shibahara K, Abe K, Ichikawa H, Valentine L, et al (2006) Increased frequency of homologous recombination and T-DNA integration in Arabidopsis CAF-1 mutants. EMBO J **25:** 5579–5590

Exner V, Taranto P, Schönrock N, Gruissem W, Hennig L (2006) Chromatin assembly factor CAF-1 is required for cellular differentiation during plant development. Development **133:** 4163–4172

Floyd SK, Bowman JL (2007) The ancestral developmental tool kit of land plants. Int J Plant Sci **168:** 1–35

Gallagher KL, Benfey PN (2009) Both the conserved GRAS domain and nuclear localization are required for SHORT-ROOT movement. Plant J **57:** 785–797

Grieneisen VA, Xu J, Marée AFM, Hogeweg P, Scheres B (2007) Auxin transport is sufficient to generate a maximum and gradient guiding root growth. Nature **449:** 1008–1013

Harberd NP, Belfield E, Yasumura Y (2009) The angiosperm gibberellin-GID1-DELLA growth regulatory mechanism: how an "inhibitor of an inhibitor" enables flexible response to fluctuating environments. Plant Cell **21:** 1328–1339

Helariutta Y, Fukaki H, Wysocka-Diller J, Nakajima K, Jung J, Sena G, Hauser MT, Benfey PN (2000) The SHORT-ROOT gene controls radial patterning of the Arabidopsis root through radial signaling. Cell **101:** 555–567

Huelsenbeck JP, Ronquist F (2001) MRBAYES: Bayesian inference of phylogenetic trees. Bioinformatics **17:** 754–755

Kaya H, Shibahara KI, Taoka KI, Iwabuchi M, Stillman B, Araki T (2001) FASCIATA genes for chromatin assembly factor-1 in Arabidopsis maintain the cellular organization of apical meristems. Cell **104:** 131–142

Kirik A, Pecinka A, Wendeler E, Reiss B (2006) The chromatin assembly factor subunit FASCIATA1 is involved in homologous recombination in plants. Plant Cell **18:** 2431–2442

Larkin MA, Blackshields G, Brown NP, Chenna R, McGettigan PA, McWilliam H, Valentin F, Wallace IM, Wilm A, Lopez R, et al (2007) Clustal W and Clustal X version 2.0. Bioinformatics **23:** 2947–2948

Laskowski M, Grieneisen VA, Hofhuis H, Hove CA, Hogeweg P, Marée AF, Scheres B (2008) Root system architecture from coupling cell shape to auxin transport. PLoS Biol **6:** e307

Laux T, Mayer KF, Berger J, Jürgens G (1996) The WUSCHEL gene is required for shoot and floral meristem integrity in Arabidopsis. Development **122:** 87–96

Llave C, Xie Z, Kasschau KD, Carrington JC (2002) Cleavage of Scarecrow-like mRNA targets directed by a class of Arabidopsis miRNA. Science **297:** 2053–2056

Long JA, Moan EI, Medford JI, Barton MK (1996) A member of the KNOTTED class of homeodomain proteins encoded by the STM gene of Arabidopsis. Nature **379:** 66–69

Lynch M (2007) The Origins of Genome Architecture. Sinauer Associates, Sunderland, MA

Mallory AC, Reinhart BJ, Jones-Rhoades M, Tang G, Zamore PD, Barton MK, Bartel DP (2004) MicroRNA control of PHABULOSA in leaf development: importance of pairing to the microRNA 5[prime] region. EMBO J **23:** 3356–3364

Matsuno M, Compagnon V, Schoch GA, Schmitt M, Debayle D, Bassard JE, Pollet B, Hehn A, Heintz D, Ullmann P, et al (2009) Evolution of a novel phenolic pathway for pollen development. Science **325:** 1688–1692

Mayer KFX, Schoof H, Haecker A, Lenhard M, Jürgens G, Laux T (1998) Role of WUSCHEL in regulating stem cell fate in the Arabidopsis shoot meristem. Cell **95:** 805–815

McConnell JR, Barton MK (1998) Leaf polarity and meristem formation in Arabidopsis. Development **125:** 2935–2942

Nakajima K, Sena G, Nawy T, Benfey PN (2001) Intercellular movement of the putative transcription factor SHR in root patterning. Nature **413:** 307–311

Ono T, Kaya H, Takeda S, Abe M, Ogawa Y, Kato M, Kakutani T, Mittelsten Scheid O, Araki T, Shibahara K (2006) Chromatin assembly factor 1 ensures the stable maintenance of silent chromatin states in Arabidopsis. Genes Cells **11:** 153–162

Ottoline Leyser HM, Furner IJ (1992) Characterisation of three shoot apical meristem mutants of Arabidopsis thaliana. Development **116:** 397–403

Parizotto EA, Dunoyer P, Rahm N, Himber C, Voinnet O (2004) In vivo investigation of the transcription, processing, endonucleolytic activity, and functional relevance of the spatial distribution of a plant miRNA. Genes Dev **18:** 2237–2242

Reinholz E (1966) Radiation induced mutants showing changed inflorescence characteristics. Arabidopsis Inf Serv **3:** 19–20

Rhoades MW, Reinhart BJ, Lim LP, Burge CB, Bartel B, Bartel DP (2002) Prediction of plant microRNA targets. Cell **110:** 513–520

Sabatini S, Heidstra R, Wildwater M, Scheres B (2003) SCARECROW is involved in positioning the stem cell niche in the Arabidopsis root meristem. Genes Dev **17:** 354–358

Samson F, Brunaud V, Balzergue S, Dubreucq B, Lepiniec L, Pelletier G, Caboche M, Lecharny A (2002) FLAGdb/FST: a database of mapped flanking insertion sites (FSTs) of Arabidopsis thaliana T-DNA transformants. Nucleic Acids Res **30:** 94–97

Schönrock N, Exner V, Probst A, Gruissem W, Hennig L (2006) Functional genomic analysis of CAF-1 mutants in Arabidopsis thaliana. J Biol Chem **281:** 9560–9568

Sozzani R, Cui H, Moreno-Risueno MA, Busch W, Van Norman JM, Vernoux T, Brady SM, Dewitte W, Murray JAH, Benfey PN (2010) Spatiotemporal regulation of cell-cycle genes by SHORTROOT links patterning and growth. Nature **466:** 128–132

Stuurman J, Jäggi F, Kuhlemeier C (2002) Shoot meristem maintenance is controlled by a GRAS-gene mediated signal from differentiating cells. Genes Dev **16:** 2213–2218

Sundaresan V, Springer P, Volpe T, Haward S, Jones JD, Dean C, Ma H, Martienssen R (1995) Patterns of gene action in plant development revealed by enhancer trap and gene trap transposable elements. Genes Dev **9:** 1797–1810

Tian C, Wan P, Sun S, Li J, Chen M (2004) Genome-wide analysis of the GRAS gene family in rice and Arabidopsis. Plant Mol Biol **54:** 519–532

Ulmasov T, Murfett J, Hagen G, Guilfoyle TJ (1997) Aux/IAA proteins repress expression of reporter genes containing natural and highly active synthetic auxin response elements. Plant Cell **9:** 1963–1971

Vazquez F, Gasciolli V, Crété P, Vaucheret H (2004) The nuclear dsRNA binding protein HYL1 is required for microRNA accumulation and plant development, but not posttranscriptional transgene silencing. Curr Biol **14:** 346–351

Vielle-Calzada JP, Thomas J, Spillane C, Coluccio A, Hoeppner MA, Grossniklaus U (1999) Maintenance of genomic imprinting at the Arabidopsis medea locus requires zygotic DDM1 activity. Genes Dev **13:** 2971–2982

Wildwater M, Campilho A, Perez-Perez JM, Heidstra R, Blilou I, Korthout H, Chatterjee J, Mariconti L, Gruissem W, Scheres B (2005) The RETINOBLASTOMA-RELATED gene regulates stem cell maintenance in Arabidopsis roots. Cell **123:** 1337–1349

Worsdell WC (1905) Fasciation: its meaning and origin. New Phytol **4:** 55–74